

Analysis of delamination growth with discontinuous solid-like shell elements

Joris J.C. Remmers*, Garth N. Wells, and René de Borst

Koiter Institute Delft / Faculty of Aerospace Engineering
Delft University of Technology, PO Box 5058, 2600 GB, Delft, The Netherlands
e-mail: J.J.C.Remmers@LR.TUDELFT.nl

Key words: partition of unity, solid-like shell element, delamination, structural stability

Abstract

In this contribution a new finite element is presented for the simulation of delamination growth in thin layered composite materials. The element is based on the solid-like shell element, a volume element that can be used in very thin applications due to a higher order displacement field in thickness direction. The delamination crack is incorporated in this element as a jump of the displacement field by means of the partition of unity method. The kinematics of the element as well as the finite element formulation are described. The performance of the element is demonstrated by means of two examples.

1 Introduction

The application of layered composite materials in the aerospace and automotive industries has increased significantly over the last decades. Since the material can be tailored to meet special demands, laminated composite structures are lighter and have superior characteristics when compared to traditional single phase materials. However, the use of these materials introduces new failure mechanisms, such as delamination, the debonding of individual layers, caused by manufacturing flaws, free edge stresses or impact damage. In general, the presence of delaminations in the material will lead to a reduction of the residual strength.

In order to get a better perception of this phenomenon, numerical simulations can be of assistance. Traditionally, in finite element models, the delamination crack is modelled explicitly by interface elements [1]. These elements consist of two surfaces which are connected to the continuum elements that model the adjoining layers of the laminate. Debonding is governed by a softening or damage algorithm.

In an alternative approach, which will be pursued here, the delamination is incorporated in the continuum elements as a discontinuity in the displacement field by means of the *partition of unity concept* [2, 3, 4, 5]. An advantage of this approach is the possibility to add new displacement jumps to the model at delamination propagation, which reduces the total number of degrees of freedom significantly. Furthermore, it avoids the use of dummy stiffnesses to simulate a perfect bond [6]. Finally, it is possible to model a complete laminate with just one continuum element in thickness direction, which allows for the analysis of delamination growth on a so-called macroscopic level [7].

In this contribution, the new method is extended to a three-dimensional model. A key feature is the choice of a proper continuum element. Conventional volume elements show an overly stiff behaviour when used in thin applications (Poisson thickness locking) due to a constant strain distribution in thickness direction. An alternative is the *solid-like shell element* [8]. Here, an additional set of internal degrees of freedom is used to add a quadratic term to the displacement field in thickness direction, the internal ‘stretch’ of the element. Hence, the corresponding strain field varies linearly over the thickness instead of being constant and Poisson thickness locking is hereby avoided.

This contribution is ordered as follows. In the next section, a short description of the kinematic relations of the original solid-like shell element is given. The derivation of the enhanced solid-like shell element with the displacement jump is presented in sections 3 and 4. Section 5 discusses a few implementation aspects. The performance of the enhanced element is demonstrated by means of two numerical examples (section 6). The contribution is closed with some conclusions.

2 Kinematics of the solid-like shell element

Consider the thick shell as shown in Figure 1. The position of a material point in the shell in the undeformed configuration can be written as a function of the three curvilinear coordinates $[\xi, \eta, \zeta]$:

$$\mathbf{X}(\xi, \eta, \zeta) = \mathbf{X}_0(\xi, \eta) + \zeta \mathbf{D}(\xi, \eta), \quad (1)$$

where $\mathbf{X}_0(\xi, \eta)$ is the projection of the point on the mid-surface of the shell and $\mathbf{D}(\xi, \eta)$ is the thickness director in this point:

$$\mathbf{X}_0(\xi, \eta) = \frac{1}{2} [\mathbf{X}_t(\xi, \eta) + \mathbf{X}_b(\xi, \eta)], \quad (2)$$

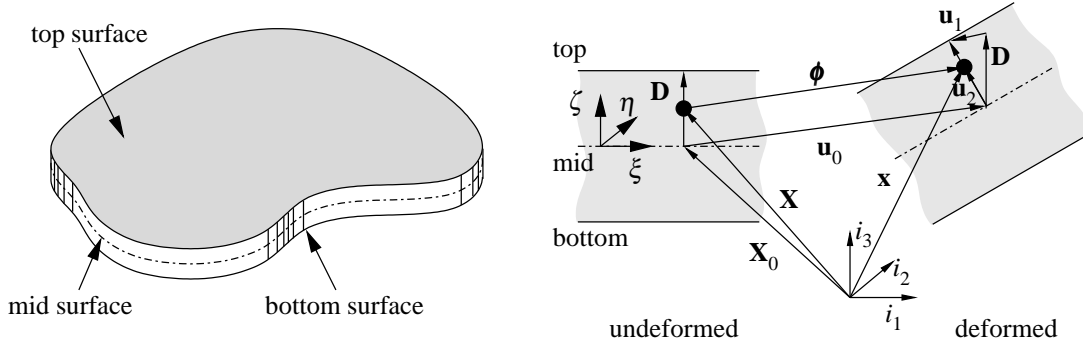


Figure 1: Kinematic relations of the regular solid-like shell element in undeformed and deformed position. The dash-dotted line denotes the mid-surface of the shell.

$$\mathbf{D}(\xi, \eta) = \frac{1}{2} [\mathbf{X}_t(\xi, \eta) - \mathbf{X}_b(\xi, \eta)]. \quad (3)$$

The subscripts $(\cdot)_t$ and $(\cdot)_b$ denote the projections of the variable onto the top and bottom surface respectively. The position of the material point in the deformed configuration $\mathbf{x}(\xi, \eta, \zeta)$ is related to $\mathbf{X}(\xi, \eta, \zeta)$ via the displacement field $\boldsymbol{\phi}(\xi, \eta, \zeta)$ according to:

$$\mathbf{x}(\xi, \eta, \zeta) = \mathbf{X}(\xi, \eta, \zeta) + \boldsymbol{\phi}(\xi, \eta, \zeta), \quad (4)$$

where:

$$\boldsymbol{\phi}(\xi, \eta, \zeta) = \mathbf{u}_0(\xi, \eta) + \zeta \mathbf{u}_1(\xi, \eta) + (1 - \zeta^2) \mathbf{u}_2(\xi, \eta). \quad (5)$$

\mathbf{u}_0 and \mathbf{u}_1 are the displacements of the shell mid-surface \mathbf{X}_0 and the thickness director \mathbf{D} respectively:

$$\mathbf{u}_0(\xi, \eta) = \frac{1}{2} [\mathbf{u}_t(\xi, \eta) + \mathbf{u}_b(\xi, \eta)], \quad (6)$$

$$\mathbf{u}_1(\xi, \eta) = \frac{1}{2} [\mathbf{u}_t(\xi, \eta) - \mathbf{u}_b(\xi, \eta)], \quad (7)$$

and $\mathbf{u}_2(\xi, \eta)$ denotes the internal stretching of the element, which is colinear with the thickness director in the deformed configuration and a function of an additional ‘stretch’ parameter w :

$$\mathbf{u}_2(\xi, \eta) = w(\xi, \eta) [\mathbf{D} + \mathbf{u}_1(\xi, \eta)], \quad (8)$$

In the remainder, we will consider the displacement field $\boldsymbol{\phi}$ as a function of three variables; the displacement vector of the top and bottom surfaces \mathbf{u}_t and \mathbf{u}_b respectively and the internal stretch parameter w :

$$\boldsymbol{\phi} = \boldsymbol{\phi}(\mathbf{u}_t, \mathbf{u}_b, w). \quad (9)$$

The displacement field will be cast in a discrete formulation for an eight-noded element¹, see Figure 2. Node numbers 1 to 4 are located at the bottom surface of the element and set up the projected displacement vector \mathbf{u}_b ; nodes 5 to 8 set up \mathbf{u}_t . The four internal degrees of freedom w^j are used to construct the

¹A description of the slightly different implementation of the sixteen-noded solid-like shell element can be found in Parisch [8].

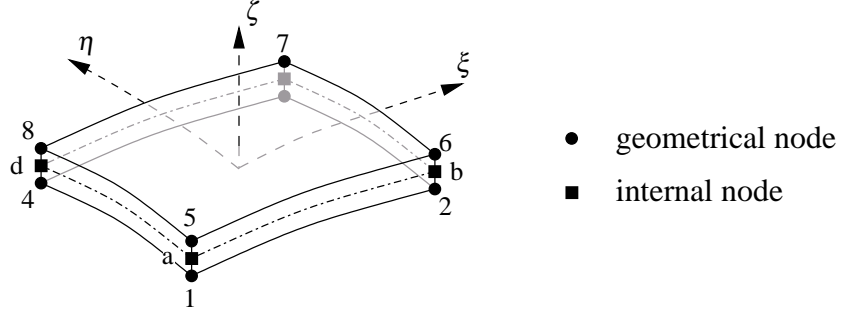


Figure 2: Geometry of the eight-noded solid-like shell element. Each geometrical node i contains three degrees of freedom: $[u_x, u_y, u_z]^i$. Each internal node j has one degree of freedom w^j .

stretch parameter w . The interpolation of these displacement parameters can be done by using standard iso-parametric shape functions [9]:

$$\mathbf{u}_t = \sum_{i=1}^4 N_i \mathbf{u}_t^i; \quad \mathbf{u}_b = \sum_{i=1}^4 N_i \mathbf{u}_b^i; \quad w = \sum_{j=1}^4 N_j w^j, \quad (10)$$

where \mathbf{u}_t^i and \mathbf{u}_b^i denote the set of three translational degrees of freedom of the nodes at the top and bottom surface respectively, w^j denotes the internal degrees of freedom.

3 Enhanced kinematic relations

Consider the thick shell with constant thickness as shown in Figure 3. The shell is crossed by a discontinuity surface $\Gamma_{d,0}$ which divides the domain into two parts, Ω_0^+ and Ω_0^- . The discontinuity surface is assumed to be parallel to the mid-surface of the thick shell. The discontinuous displacement field $\boldsymbol{\phi}(\xi, \eta, \zeta)$ can be decomposed in two parts [5], so that the position of a material point in the deformed configuration can be written as:

$$\mathbf{x} = \mathbf{X} + \hat{\boldsymbol{\phi}} + \mathcal{H}_{\Gamma_{d,0}} \tilde{\boldsymbol{\phi}}, \quad (11)$$

where $\mathcal{H}_{\Gamma_{d,0}}$ represents the Heaviside step function, which is defined as $\mathcal{H}_{\Gamma_{d,0}}(\mathbf{X}) = 1$ if $\mathbf{X} \in \Omega_0^+$ and $\mathcal{H}_{\Gamma_{d,0}}(\mathbf{X}) = 0$ if $\mathbf{X} \in \Omega_0^-$. Since the displacement field is just a function of \mathbf{u}_t , \mathbf{u}_b and w , it is sufficient to enhance these terms:

$$\mathbf{u}_t = \hat{\mathbf{u}}_t + \mathcal{H}_{\Gamma_{d,0}} \tilde{\mathbf{u}}_t; \quad \mathbf{u}_b = \hat{\mathbf{u}}_b + \mathcal{H}_{\Gamma_{d,0}} \tilde{\mathbf{u}}_b; \quad w = \hat{w} + \mathcal{H}_{\Gamma_{d,0}} \tilde{w}. \quad (12)$$

Inserting these relations into Eqs. (6) to (8) gives:

$$\mathbf{u}_0 = \hat{\mathbf{u}}_0 + \mathcal{H}_{\Gamma_{d,0}} \tilde{\mathbf{u}}_0; \quad \mathbf{u}_1 = \hat{\mathbf{u}}_1 + \mathcal{H}_{\Gamma_{d,0}} \tilde{\mathbf{u}}_1; \quad \mathbf{u}_2 = \hat{\mathbf{u}}_2 + \mathcal{H}_{\Gamma_{d,0}} \tilde{\mathbf{u}}_2, \quad (13)$$

where:

$$\begin{aligned} \hat{\mathbf{u}}_0 &= \frac{1}{2} [\hat{\mathbf{u}}_t + \hat{\mathbf{u}}_b] & \tilde{\mathbf{u}}_0 &= \frac{1}{2} [\tilde{\mathbf{u}}_t + \tilde{\mathbf{u}}_b] \\ \hat{\mathbf{u}}_1 &= \frac{1}{2} [\hat{\mathbf{u}}_t - \hat{\mathbf{u}}_b] & \tilde{\mathbf{u}}_1 &= \frac{1}{2} [\tilde{\mathbf{u}}_t - \tilde{\mathbf{u}}_b] \\ \hat{\mathbf{u}}_2 &= \hat{w} [\mathbf{D} + \hat{\mathbf{u}}_1] & \tilde{\mathbf{u}}_2 &= \tilde{w} [\mathbf{D} + \hat{\mathbf{u}}_1 + \tilde{\mathbf{u}}_1] + \tilde{w} \tilde{\mathbf{u}}_1 \end{aligned} \quad (14)$$

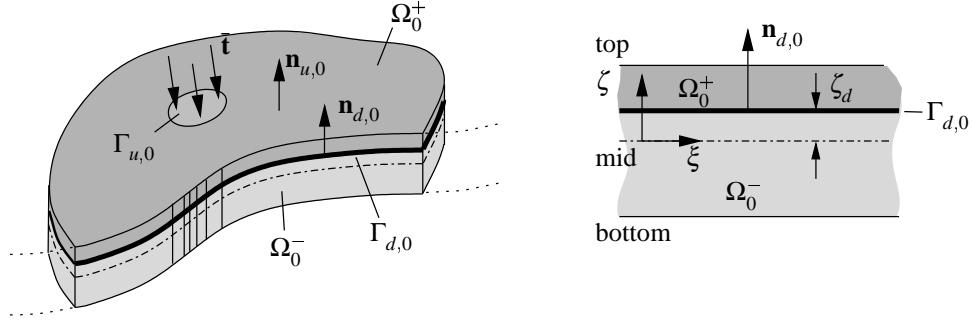


Figure 3: Thick shell crossed by a discontinuity $\Gamma_{d,0}$ (heavy line). The vectors $\mathbf{n}_{u,0}$ and $\mathbf{n}_{d,0}$ are perpendicular to the shell surface and the discontinuity surface respectively.

Note that the enhanced part of the internal stretch parameter \mathbf{u}_2 contains both regular and enhanced variables.

The base vectors at the material point in undeformed and deformed configuration can be found by differentiating the position vectors \mathbf{X} and \mathbf{x} with respect to the iso-parametric coordinates $\Theta^i = [\xi, \eta, \zeta]$. In the undeformed configuration, the base vectors are equal to:

$$\mathbf{G}_\alpha = \frac{\partial \mathbf{X}}{\partial \Theta^\alpha} = \mathbf{X}_{0,\alpha} + \zeta \mathbf{D}_{,\alpha} \quad \alpha = 1, 2, \quad (15)$$

$$\mathbf{G}_3 = \frac{\partial \mathbf{X}}{\partial \Theta^3} = \mathbf{D} \quad , \quad (16)$$

where $(\cdot)_{,\alpha}$ denotes the partial derivative with respect to Θ^α . In the deformed configuration, the base vectors in the ξ and η direction are equal to:

$$\mathbf{g}_\alpha = \mathbf{X}_{0,\alpha} + \hat{\mathbf{u}}_{0,\alpha} + \zeta \mathbf{D}_{,\alpha} + \zeta \hat{\mathbf{u}}_{1,\alpha} + \mathcal{H}_{\Gamma_{d,0}} [\tilde{\mathbf{u}}_{0,\alpha} + \zeta \tilde{\mathbf{u}}_{1,\alpha}] + \text{h.o.t.} \quad \forall \zeta \neq \zeta_d, \quad (17)$$

whereas the base vector in the deformed configuration in the ζ direction is:

$$\mathbf{g}_3 = \mathbf{D} + \hat{\mathbf{u}}_1 - 2\zeta \hat{\mathbf{w}} + \mathcal{H}_{\Gamma_{d,0}} [\tilde{\mathbf{u}}_1 - 2\zeta \tilde{\mathbf{w}}] + \text{h.o.t.} \quad \forall \zeta \neq \zeta_d. \quad (18)$$

The higher order terms (h.o.t.) in these expressions contain terms up to the fourth order in the thickness coordinate ζ and derivatives of the stretch parameter \mathbf{u}_2 with respect to ξ and η . In the continuing, these terms will be neglected without a significant loss of accuracy of the kinematic model [8].

The metric tensors \mathbf{G} and \mathbf{g} can be determined by using the base vectors \mathbf{G}_i and \mathbf{g}_i in Eqs. (15) to (18):

$$G_{ij} = \mathbf{G}_i \cdot \mathbf{G}_j; \quad g_{ij} = \mathbf{g}_i \cdot \mathbf{g}_j. \quad (19)$$

The metric tensors in turn are used to determine the Green-Lagrange strain tensor $\boldsymbol{\gamma}$, according to:

$$\gamma_{kl} = \frac{1}{2} (g_{ij} - G_{ij}) \mathbf{t}_k^i \mathbf{t}_l^j, \quad (20)$$

where the tensor \mathbf{t}_j^i denotes the transformation of the strains in the element iso-parametric coordinate system into the global frame of reference. The strain tensor can be divided into a regular and an additional part as well:

$$\boldsymbol{\gamma} = \hat{\boldsymbol{\gamma}} + \mathcal{H}_{\Gamma_{d,0}} \tilde{\boldsymbol{\gamma}}. \quad (21)$$

Note that the strain fields on either side of the discontinuity $\Gamma_{d,0}$ are not necessarily equal. This implies that it is possible to capture phenomena which are restricted to just one layer of the laminate such as delamination buckling [10].

The magnitude of the displacement jump \mathbf{v} is equal to the magnitude of the enhanced displacement at the discontinuity ζ_d . In the spirit of previous assumptions, we neglect the terms that vary quadratically in the thickness direction.

$$\mathbf{v} = \tilde{\mathbf{u}}_0 + \zeta_d \tilde{\mathbf{u}}_1. \quad (22)$$

4 Equilibrium equations

The static equilibrium equations and boundary conditions for the body Ω without body forces with respect to the undeformed configuration can be written as:

$$\nabla_0 \cdot \mathbf{P} = 0 \quad \text{in } \Omega_0; \quad (23a)$$

$$\mathbf{n}_{u,0} \mathbf{P} = \bar{\mathbf{t}} \quad \text{on } \Gamma_{u,0}; \quad (23b)$$

$$\mathbf{n}_{d,0} \mathbf{P} = \mathbf{t} \quad \text{on } \Gamma_{d,0}, \quad (23c)$$

where \mathbf{P} is the nominal stress tensor and $\bar{\mathbf{t}}$ the applied external load; $\mathbf{n}_{u,0}$ is the outward unit normal vector to the body and $\mathbf{n}_{d,0}$ is the inward unit normal to Ω_0^+ , see also Figure 3. Eq. (23c) represents the tractions at the discontinuity $\Gamma_{d,0}$ and is a functional of the displacement jump \mathbf{v} :

$$\mathbf{t} = \mathcal{F}(\mathbf{v}). \quad (24)$$

The strong governing equations can be written as the weak equations of equilibrium by multiplying Equation (23a) with an admissible displacement field $\boldsymbol{\phi}$ and integrating the result over the domain Ω_0 :

$$\int_{\Omega_0} \delta \boldsymbol{\phi} \cdot (\nabla_0 \cdot \mathbf{P}) d\Omega_0 = 0. \quad (25)$$

The admissible displacement field must have the same format as the standard displacement field:

$$\delta \boldsymbol{\phi} = \delta \hat{\boldsymbol{\phi}} + \mathcal{H}_{\Gamma_{d,0}} \delta \tilde{\boldsymbol{\phi}}. \quad (26)$$

Substituting this relation into Eq. (25) gives:

$$\int_{\Omega_0} \delta \hat{\boldsymbol{\phi}} \cdot (\nabla_0 \cdot \mathbf{P}) d\Omega_0 + \int_{\Omega_0} \mathcal{H}_{\Gamma_{d,0}} \delta \tilde{\boldsymbol{\phi}} \cdot (\nabla_0 \cdot \mathbf{P}) d\Omega_0 = 0. \quad (27)$$

This equation can be separated into two equations by taking first variation $\hat{\boldsymbol{\phi}}$ ($\tilde{\boldsymbol{\phi}} = 0$) and then variation $\tilde{\boldsymbol{\phi}}$ ($\hat{\boldsymbol{\phi}} = 0$). The separated equations can be expanded by using Gauss' theorem. The Heaviside function can be eliminated by changing the integration domain Ω_0 into Ω_0^+ [5, 11]:

$$\int_{\Omega_0} \delta \hat{\boldsymbol{\phi}} \cdot (\nabla_0 \cdot \mathbf{P}) d\Omega_0 = \int_{\Omega_0} \nabla_0 \cdot (\mathbf{P} \delta \hat{\boldsymbol{\phi}}) d\Omega_0 - \int_{\Omega_0} \nabla_0 \delta \hat{\boldsymbol{\phi}} : \mathbf{P} d\Omega_0 = 0, \quad (28a)$$

$$\int_{\Omega_0} \mathcal{H}_{\Gamma_{d,0}} \delta \tilde{\boldsymbol{\phi}} \cdot (\nabla_0 \cdot \mathbf{P}) d\Omega_0 = \int_{\Omega_0^+} \nabla_0 \cdot (\mathbf{P} \delta \tilde{\boldsymbol{\phi}}) d\Omega_0 - \int_{\Omega_0^+} \nabla_0 \delta \tilde{\boldsymbol{\phi}} : \mathbf{P} d\Omega_0 = 0. \quad (28b)$$

By using the boundary conditions in Eqs. (23b) and (23c), the two equilibrium equations can be written as:

$$\int_{\Omega_0} \nabla_0 \delta \hat{\boldsymbol{\phi}} : \mathbf{P} \, d\Omega_0 = \int_{\Gamma_{u,0}} \delta \hat{\boldsymbol{\phi}} \cdot \bar{\mathbf{t}} \, d\Gamma_0 \quad (29a)$$

$$\int_{\Omega_0^+} \nabla_0 \delta \tilde{\boldsymbol{\phi}} : \mathbf{P} \, d\Omega_0 + \int_{\Gamma_{d,0}} \delta \tilde{\boldsymbol{\phi}} \cdot \mathbf{t} \, d\Omega_0 = \mathcal{H}_{\Gamma_{d,0}} \int_{\Gamma_{u,0}} \delta \tilde{\boldsymbol{\phi}} \cdot \bar{\mathbf{t}} \, d\Gamma_0. \quad (29b)$$

The terms $\nabla_0 \delta \hat{\boldsymbol{\phi}} : \mathbf{P}$ and $\nabla_0 \delta \tilde{\boldsymbol{\phi}} : \mathbf{P}$ can be replaced by $\delta \hat{\boldsymbol{\gamma}} : \boldsymbol{\sigma}$ and $\delta \tilde{\boldsymbol{\gamma}} : \boldsymbol{\sigma}$ respectively [12], where $\boldsymbol{\sigma}$ is the second Piola-Kirchhoff stress tensor:

$$\int_{\Omega_0} \delta \hat{\boldsymbol{\gamma}} : \boldsymbol{\sigma} \, d\Omega_0 = \int_{\Gamma_{u,0}} \delta \hat{\boldsymbol{\phi}} \cdot \bar{\mathbf{t}} \, d\Gamma_0, \quad (30a)$$

$$\int_{\Omega_0^+} \delta \tilde{\boldsymbol{\gamma}} : \boldsymbol{\sigma} \, d\Omega_0 + \int_{\Gamma_{d,0}} \delta \tilde{\boldsymbol{\phi}} \cdot \mathbf{t} \, d\Omega_0 = \mathcal{H}_{\Gamma_{d,0}} \int_{\Gamma_{u,0}} \delta \tilde{\boldsymbol{\phi}} \cdot \bar{\mathbf{t}} \, d\Gamma_0. \quad (30b)$$

These equilibrium equations still hold for large strains. For engineering purposes, when nonlinear material models for the bulk material are implemented, a small strain formulation may be preferred.

5 Finite element implementation

The discontinuous displacement field can be written in a discrete form by using the standard finite element shape functions. It was shown by Babuška *et al.* [2] that the basis of the finite element shape functions can be enriched with enhanced bases. This means that when ψ_i is a partition of unity, a field u can be interpolated in terms of nodal values according to:

$$u(\mathbf{X}, t) = \sum_{i=1}^n \psi_i(\mathbf{X}) \left(a^i(t) + \sum_{j=1}^m \beta_j(\mathbf{X}) b^{ij}(t) \right). \quad (31)$$

In this specific case, the function β_j can be replaced by the Heaviside step function $\mathcal{H}_{\Gamma_{d,0}}$ and ψ_i by the standard iso-parametric shape functions; a^i represent the regular nodal degrees of freedom and b^{ij} the additional nodal degrees of freedom. Since the displacement field is constructed with three different sets of degrees of freedom, see Eq. (10), all sets can be enhanced independently. For the eight-noded element, the new discrete displacement fields are:

$$\mathbf{u}_t = \sum_{i=1}^4 N_i \hat{\mathbf{u}}_t^i + \mathcal{H}_{\Gamma_{d,0}} \sum_{i=1}^4 N_i \tilde{\mathbf{u}}_t^i; \quad \mathbf{u}_b = \sum_{i=1}^4 N_i \hat{\mathbf{u}}_b^i + \mathcal{H}_{\Gamma_{d,0}} \sum_{i=1}^4 N_i \tilde{\mathbf{u}}_b^i; \quad w = \sum_{i=j}^4 N_j \hat{w}^j + \mathcal{H}_{\Gamma_{d,0}} \sum_{i=j}^4 N_j \tilde{w}^j. \quad (32)$$

The interpolation of the nodal values of the sixteen-noded enhanced solid-like shell element can be derived in a similar fashion [13].

Enhancement of geometrical and internal nodes

Figure 4 shows the activation of additional sets of degrees of freedom for a given delamination surface in the model. Both the geometrical and the internal nodes are enhanced when the element is crossed by a delamination. This implies that each geometrical node contains 3 additional degrees of freedom giving 6 degrees of freedom in total. Each internal node has one extra degree of freedom added to the single regular degree of freedom.

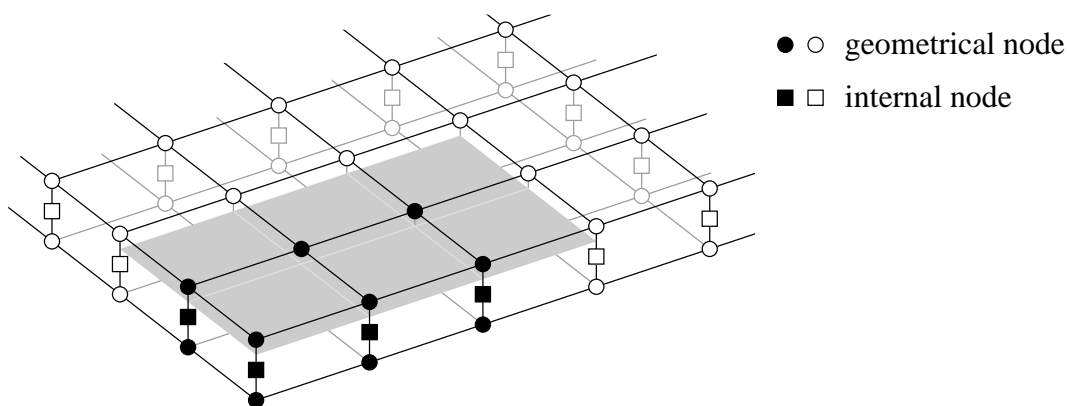


Figure 4: Enhanced nodes (black) whose support contains a discontinuity (grey surface). The nodes on the edge of the discontinuity are not enhanced in order to assure a zero delamination opening here.

A displacement jump is added to an element when the stress state at the interface of two layers within the element exceeds an ultimate level. It is assumed that the delamination crosses an entire element avoiding the need of complicated stress concentration algorithms to describe the stress state in the vicinity of the delamination front. The degrees of freedom that support the edge of the elements that touch the delamination front are not enhanced in order to assure a zero crack tip condition, see also Fig. 4.

Condensation of the internal degrees of freedom

The original eight-noded solid-like shell element consists of 28 degrees of freedom; 3 translational degrees of freedom in the eight geometrical nodes and 4 internal degrees of freedom. Since the internal degrees of freedom are not able to support an external loading, it was suggested by Parisch to eliminate them on the element level by condensation [8].

It is emphasised that the additional degrees of freedom that describe the displacement jump cannot be condensed. The magnitude of the displacement jump is continuous across element boundaries. The degrees of freedom that describe this jump are therefore global and cannot be solved on the element local level. An exception is made for the additional internal degrees of freedom \tilde{w}^j [13]. Since the regular internal degrees of freedom \hat{w}^j are not continuous across element boundaries, there is no need for the additional internal degrees of freedom to be continuous. In practice, an enhanced eight-noded solid-like shell element has a total of 56 degrees of freedom; 2 times 3 in each geometrical node plus 2 times 4 internal degrees of freedom. These last 2 sets are eliminated by condensation reducing the contribution of the element to the global solution vector to 48 degrees of freedom.

Numerical integration

The construction of the element internal force vector and stiffness matrix requires a proper integration of three domains; Ω_0 , Ω_0^+ and $\Gamma_{d,0}$, see also Eq. (30). In this case, all three domains are standard geometrical entities (two six-sided volumes and a rectangular surface) and can be integrated numerically with standard Gauss integration schemes.

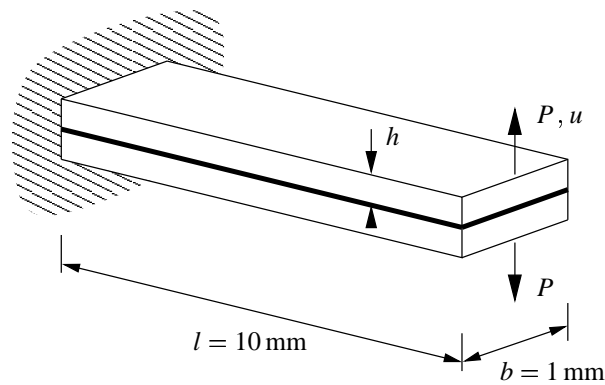


Figure 5: Geometry of a delaminated double cantilever beam under peel loading.

6 Numerical examples

Two examples are presented to demonstrate the performance of the new element. In the first example, attention is focused on the accuracy of the element for a decreasing thickness in geometrically linear applications. In the second example, the performance of the element in a geometrically nonlinear analysis is illustrated by means of the simulation of a delamination buckling test.

A peel test

To test the performance of the new element for a decreasing thickness, a peel test is performed. Consider the double cantilever beam as shown in Figure 5. The beam consists of two layers of the same material with Young's modulus $E = 100.0 \text{ N/mm}^2$ and Poisson ratio 0.0. The beam has delaminated over its entire length. The test is performed for two different models. The first model contains ten eight-noded enhanced solid-like shell elements (SLS+8); the second model is built with just five sixteen-noded enhanced solid-like shell elements (SLS+16). In both cases, just one element in thickness direction is used. The initial delamination is modelled by a traction free discontinuity.

The linear out-of-plane displacements as functions of the ratio of layer thickness and beam length are given in Figure 6. The results are normalised by the exact solution that follows from the theory of beam deflections. The eight-noded enhanced solid-like shell element gives nearly exact results for aspect ratios up to 2000. The performance of the new sixteen-noded element is even better. Both results are identical to the results with original solid-like shell elements [8]. It can therefore be concluded that kinematic properties of the new enhanced solid-like shell elements are identical to those of the original elements.

Delamination buckling of a cantilever beam

A combination of delamination growth and structural instability is considered in the following example [7, 14]. Consider the double cantilever beam as shown in Figure 7. The beam has an initial delamination length of $a_0 = 10 \text{ mm}$ and is subjected to an axial compressive load $2P$. Two small perturbation forces P_0 are applied to trigger the desired buckling mode. Both layers are made of the same material with Young's modulus $E = 135000 \text{ N/mm}^2$ and Poisson's ratio $\nu = 0.18$. The ultimate strength of the bond in mode-I is equal to $t_{I,ult} = 50 \text{ N/mm}^2$, the fracture toughness is $G_c = 0.8 \text{ N/mm}$. The critical load for local buckling of the beam, prior to delamination growth can be calculated analytically using the

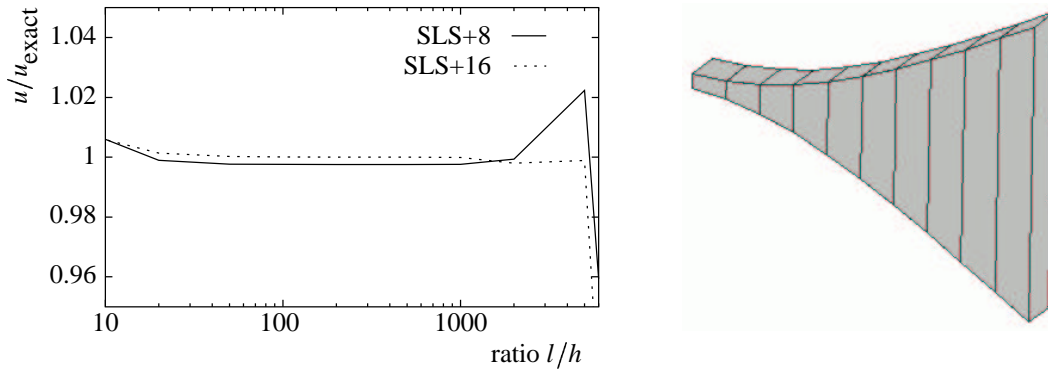


Figure 6: Double cantilever beam loaded by peel force. Left: Normalised linear solution as a function of the length over layer thickness ratio. Right: deformed mesh.

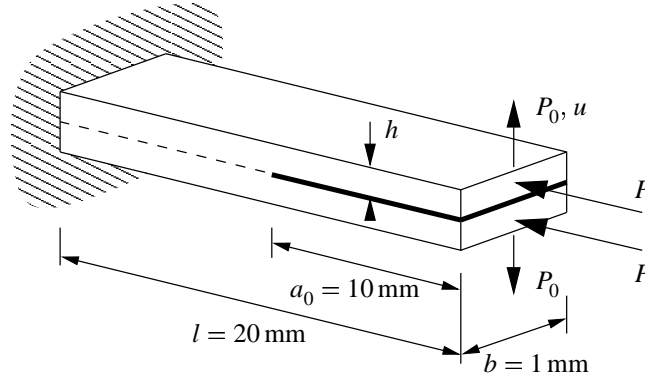


Figure 7: Geometry of double cantilever beam with initial delamination a_0 under compression.

equation for a single cantilever beam with length a_0 and thickness h . For the given material parameters, the buckling load is:

$$P_{\text{cr}} = \frac{\pi^2 E h^3}{48 a_0^2} = 2.22 \text{ N} \quad (33)$$

The finite element mesh used for the analysis is made of eight-noded enhanced solid-like shell elements and is shown in Figure 8. Again, it consists of just one element in thickness direction. In order to capture delamination growth correctly, the mesh is locally refined.

Figure 8 shows the lateral displacement u of the beam as a function of the external force P . The load-displacement curve for a specimen with a perfect bond (no delamination) is given as a reference. The numerically calculated buckling load is in agreement with the analytical solution. Steady delamination growth starts at a lateral displacement $u = 4 \text{ mm}$, which is in agreement with previous simulations [14].

7 Conclusions

In this contribution, a new element for the simulation of delamination growth in thin layered composite materials is presented. The delamination crack is incorporated in the solid-like shell element by means of the partition of unity concept. The approach has a number of advantages. First, the displacement jump is only activated as the delamination propagates, which results in a reduction of the total number of degrees

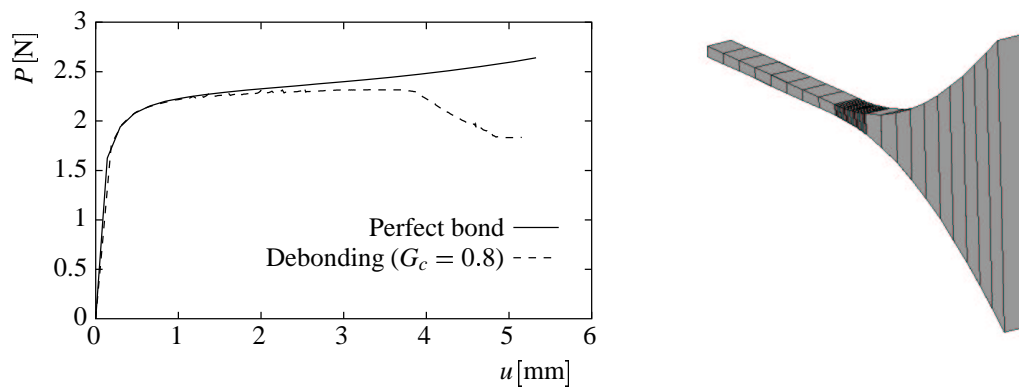


Figure 8: Delamination buckling test. Left: tip displacement as a function of the applied axial load P . Right: final deformation.

of freedom. Besides that, it is possible to model a laminate with a delamination with just one element in thickness direction, whereas with conventional techniques, at least the double amount of elements is needed. This last property allows to use coarser meshes and analyse delamination phenomena on a macroscopic level.

It has been shown that the new element has the same kinematic characteristics as the conventional solid-like shell element. It can still be used in thin application without showing an overly stiff behaviour. A delamination buckling example underlines the excellent performance of the element in combined geometrically and physically nonlinear analyses.

References

- [1] G. Alfano, M. Crisfield, *Finite element interface models for the delamination analysis of laminated composites: mechanical and computational issues*, International Journal for Numerical Methods in Engineering, 50 (7), (2001), 1701–1736.
- [2] I. Babuška, J. Melenk, *The partition of unity method*, International Journal for Numerical Methods in Engineering, 40 (4), (1997), 727–758.
- [3] T. Belytschko, T. Black, *Elastic crack growth in finite elements with minimal remeshing*, International Journal for Numerical Methods in Engineering, 45 (5), (1999), 601–620.
- [4] N. Moës, J. Dolbow, T. Belytschko, *A finite element method for crack growth without remeshing*, International Journal for Numerical Methods in Engineering, 46 (1), (1999), 131–150.
- [5] G. Wells, L. Sluys, *A new method for modelling cohesive cracks using finite elements*, International Journal for Numerical Methods in Engineering, 50 (12), (2001), 2667–2682.
- [6] J. Schellekens, R. de Borst, *On the numerical integration of interface elements*, International Journal for Numerical Methods in Engineering, 36, (1993), 43–66.
- [7] G. Wells, J. Remmers, R. de Borst, L. Sluys, *A large strain discontinuous finite element approach to laminated composites*, Kluwer, Dordrecht (2002), proceedings of IUTAM Symposium on Computational Mechanics of Solid Materials at Large Strains.

- [8] H. Parisch, *A continuum-based shell theory for non-linear applications*, International Journal for Numerical Methods in Engineering, 38 (11), (1995), 1855–1883.
- [9] O. Zienkiewicz, R. Taylor, *The Finite Element Method, Vol. 1, Basic Formulation and Linear Problems*, Mc-Graw Hill (1989).
- [10] G. Wells, R. de Borst, L. Sluys, *A consistent geometrically non-linear approach for delamination* (2002), International Journal for Numerical Methods in Engineering (in print).
- [11] A. Simone, J. Remmers, G. Wells, *Modelling interface phenomena with enriched finite elements* (2002), submitted to Computer Methods in Applied Mechanics and Engineering.
- [12] T. Belytschko, W. Liu, B. Moran, *Nonlinear Finite Elements for Continua and Structures*, John Wiley and Sons Ltd. (2000).
- [13] J. Remmers, G. Wells, R. de Borst, *A discontinuous solid-like shell element for the analysis of delamination growth in laminated composite materials* (2002), submitted to International Journal for Numerical Methods in Engineering.
- [14] O. Allix, A. Corigliano, *Geometrical and interfacial non-linearities in the analysis of delamination in composites*, International Journal of Solids and Structures, 36 (15), (1999), 2189–2216.